Online ISSN: 2981-0396 Print ISSN: 2981-0388

International Journal of Iron & Steel Society of Iran

Journal Homepage: https://journal.issiran.com/

Research Article

Corrosion performance of an additive manufactured 316L stainless steel in the concrete pore solution

M. Yeganeh *[1], M. H. Shaeri Karimi [2], S. R. Alavi Zaree [3], M. Eskandari [4]

Department of Materials Science and Engineering, Faculty of Engineering, Shahid Chamran University of Ahvaz, Ahvaz, Iran

ARTICLE INFO

Keywords:

Additive manufacturing, Selective laser melting, 316L SS, Corrosion, Concrete pore solution.

Article history:

Received 05 October 2022
Received in revised form 14 August 2023
Accepted 26 August 2023

ABSTRACT

Selective laser melting (SLM) is a manufacturing technique that can be used to create products with complex geometries and materials. This study investigated the microstructure and electrochemical behavior of SLM-processed 316L stainless steel (SLM-fabricated 316L SS) and a commercially wrought counterpart in a concrete pore solution. The results showed that SLMed 316L SS had a finer microstructure with ultrafine cellular/columnar grains than the wrought counterpart. This was due to the high cooling rate of the SLM process. The SLM sample also had a higher charge transfer resistance and lower corrosion current densities than the wrought counterpart, indicating better corrosion performance in alkaline media. This could be attributed to the fabrication method of the SLM- fabricated sample, which prevents the formation of harmful phases and defects.

1. Introduction

Additive manufacturing (AM) of alloys has been a subject of significant interest due to its ability to produce intricate pieces. In recent years, the mechanical properties of AM products have improved as defects have decreased and mechanical properties have been enhanced [1]. Additive manufacturing (AM) alloys have finer microstructures than conventional fabrication processes such as casting and rolling due to the rapid cooling of the molten alloy during fabrication. This rapid cooling also increases the solubility of the elements in the alloy matrix, which can further improve the mechanical properties of the AM alloy. As a result, AM specimens often have higher mechanical properties than conventionally manufactured specimens [2]. Stainless steel (SS) alloys are manufactured using AM techniques due to their exceptional mechanical and corrosion properties. 316L stainless steel is a versatile alloy with excellent characteristics, making it suitable for a wide range of applications [3–7].

It has recently been found that selective laser melting (SLM) technology can be used to create products with near-net-shape, complex, or functionally graded geometries and materials [8, 9]. Furthermore, products fabricated using selective laser melting (SLM) technology offer mechanical properties that are comparable to those of products produced using conventional methods with full density [10, 11]. The selective laser melting (SLM) process produces a microstructure that differs greatly from cast or wrought products due to its extremely high cooling rate [12]. In the building direction, selective laser melting (SLM) forms circular melt pools with overlapping melt pools. The reported microstructure of SLMed alloy is mainly determined by a cellular/columnar sub-grains. The microstructure of these sub-grain boundaries is very

*Corresponding author
Email: m.yeganeh@scu.ac.ir
Address: Department of Materials Science and Engineering, Faculty of Engineering, Shahid Chamran University of Ahvaz, Ahvaz, Iran
1. Associate professor, 2. M.S. Student, 3. Associate professor, 4. Associate professor

http://10.22034/IJISSI.2023.562806.1251
Published by ISSI (Iron & Steel Society of Iran)

fine [13, 14].

The investigation of the corrosion resistance of SLM-fabricated 316L stainless steel has gained much interest in recent years. Some researchers have found that 316L stainless steel manufactured by additive manufacturing (AM) is more corrosion resistant than its traditional counterparts [15, 16]. he high corrosion resistance of AM 316L SS sample was attributed to the ultrafine grain structure created by the rapid quenching of the alloy powders after laser melting [17]. Passive films developed on stainless steel can be more stable in corrosive media because of their fine cellular/columnar structure [18]. The laser melting process also prevents the formation of harmful MnS or (Ca,Al)-oxides [15].

In this study, long term corrosion behavior of SLM-fabricated 316L SS investigated in the concrete pore solution by potentiodynamic polarization and electrochemical impedance spectroscopy (EIS). Although the microstructure of as-received and corroded samples has been studied by scanning electron microscopy equipped with energy dispersive x-ray spectroscopy (EDS).

2. Experimental

2.1. Materials

The SLM-fabricated parts in the study you mentioned were manufactured with 316L stainless steel gas atomized powder with a maximum particle size of 65 µm. The stainless steel powders were melted with a fiber laser of 300 watts and a hatch distance of 100 µm. During the SLM process, each melted layer was set at a thickness of 30 µm. After the SLM process was carried out in an atmosphere of argon gas, cubes of 25×20×2 mm were manufactured. The schematic in Fig. 1a and 1b depicts the selective laser melting (SLM) process for producing 3D printed specimens (Fig. 1a.) and cubes (Fig. 1b.). A commercially wrought 316L stainless steel plate was provided for comparison. The chemical composition of both wrought and SLM-fabricated 316L SS confirms that the alloy belongs to the austenitic stainless steel group, as previously reported [6, 19, 20]. In addition, Mojallali Co. Iran provided analytical grade powders of sodium chloride (NaCl), sodium hydroxide (NaOH), and oxalic acid ($C_2H_2O_4$).

2.2. Methods

Samples of 316L SS that were fabricated using Wrought and SLM techniques were ground with SiC sandpapers, up to a size of 2000 grit. Afterward, they were degreased in acetone, cleansed in distilled water, and dried using cold air. The samples were then connected to a copper wire and mounted using an epoxy resin for electrochemical tests. In addition, the polished samples underwent electro-etching in a solution containing 10 g oxalic acid and 100 cc deionized water with the application of 6 V for 30 s [19]. The surface micrographs of the stainless steel samples that were both wrought and SLMed were examined using a field emission scanning electron microscope (Camscan Mira Model). The distribution of elements in the steel alloy was also analyzed using an EDS detector.

To conduct electrochemical corrosion studies, a three-electrode cell system was used, with either wrought or SLMed samples serving as the working electrode. These samples were mounted with epoxy resin and exposed to a concrete pore solution containing 0.9 M NaOH and 0.9 wt.% NaCl. A Pt wire and an Ag/AgCl electrode acted as the counter and reference electrodes, respectively. Electrochemical analyses were carried out using a Radstat 1A potentiostat, including electrochemical impedance spectroscopy (EIS) and potentiodynamic polarization to analyze the electrochemical behavior of the specimens in the concrete pore solution. EIS measurements were taken at OCP at different times in a frequency range of 10 kHz to 10 mHz with an applied AC signal of 5 mV. The experimental results were analyzed using ZView 3.1 software and electrochemical equivalent circuits to measure the corrosion parameters. Polarization parameters including corrosion current density (i_{corr}), corrosion potential (E_{corr}), cathodic and anodic slopes (βc and βa), potential of passivation (E_{pass}), and potential of pitting (E_{pit}) were obtained using the Tafel extrapolation method.

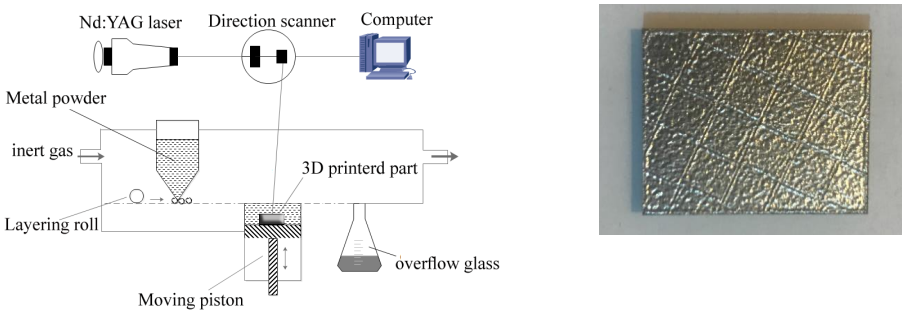

(a) (b)

Fig. 1. (a) Schematic process of SLM process to produce 3D printed 316L SS [19] and (b) the produced cubes (the length of cube is 25 mm).

3. Results and discussion

The microstructure of wrought and SLMed 316L SS was examined using optical and FESEM micrographs. Wrought alloy (Fig. 2a.) has an angular morphology, sharp edges with a grain size of about 25 µm, while SLM-fabricated specimen (Fig. 2b.) shows a heterogeneous structure with overlapping oval melt pools and cellular/columnar sub-grains. The size of each cell is determined by the temperature gradient and cooling rate, which in the SLM process with high cooling rates leads to ultrafine grains [19].

The surface micrographs in Fig. 3 a-b. illustrate the presence of inclusions in both the wrought (a-b) and SLMed (c-d) 316L SS. The wrought alloy contains sharp inclusions, while the SLM-fabricated counterpart has spherical inclusions. The main elements present in the inclusions of the wrought sample are Ti and N, whereas those in the SLM-fabricated sample are Mn, Si, Cr, and O. The inclusion compositions in the wrought sample is TiN, which can lead to pitting due to the formation of galvanic couples between TiN particles and the matrix [7, 21]. In contrast, the inclusions in the SLM-fabricated sample are probably combinations of metallic oxides that precipitate during solidification. These oxide inclusions have a round shape and are not as detrimental as those in the wrought samples.

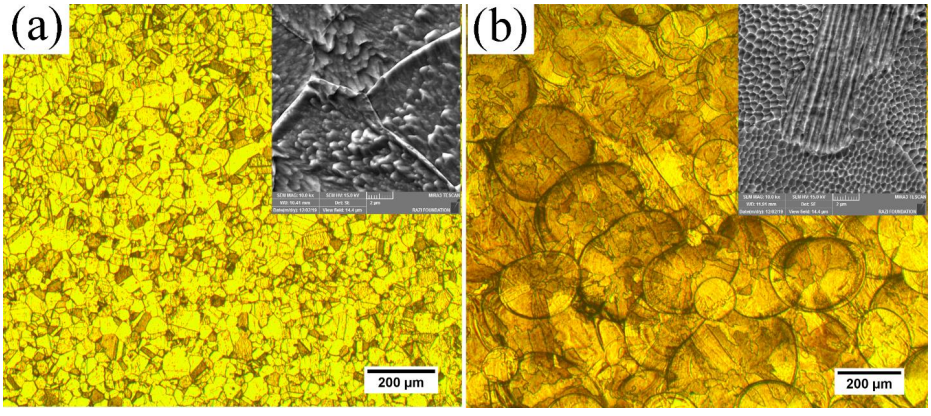

Fig. 2. FESEM micrographs of 316L stainless steel (a) wrought, (b) SLM fabricated one.

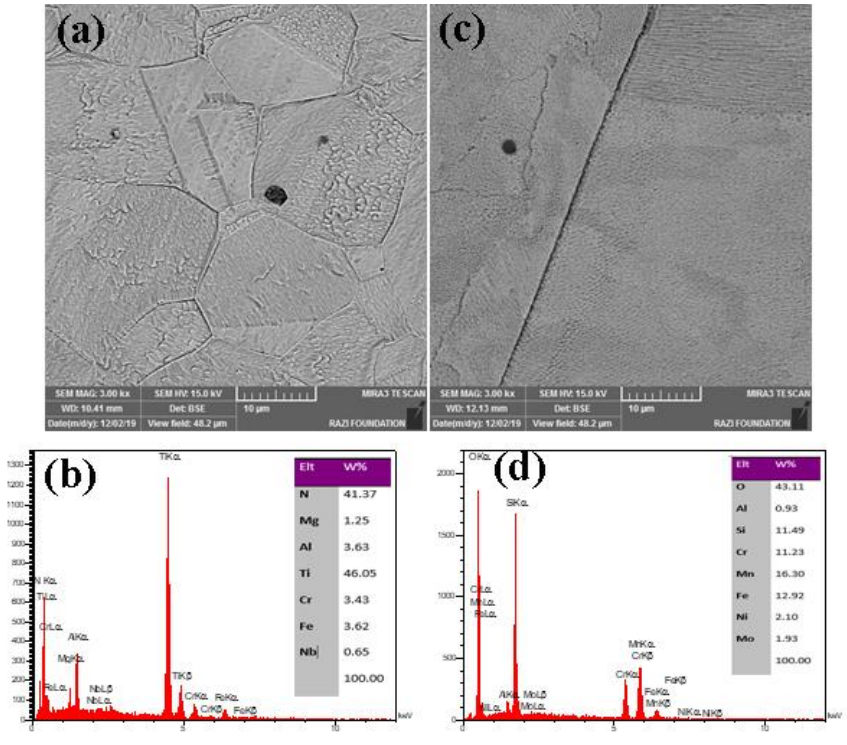

Fig. 3. SEM micrographs and EDS related to inclusion in the (a, b) wrought sample, and (c, d) SLM manufactured sample.

The corrosion behavior of 316L SS samples, both wrought and SLM processed, in concrete pore solution after 3 hours of immersion is depicted in Fig. 4a. through Nyquist plots. These plots represent the electrochemical behavior of metal/electrolyte through a depressed capacitive semi-circle. The radius of the semi-circle indicates the charge transfer resistance of the samples [22]. The inserted circuit in Fig. 4a. can be used to explain the corroded samples' electrochemical behavior in the concrete pore solution. Experimental data was simulated using ZView software based on electrochemical phenomena. The inserted circuit used to explain the corroded samples' electrochemical behavior includes a solution resistance, R_s, a charge transfer resistance, R_{dl}, and a constant phase element of charge transfer resistance, CPE_{dl}. R_s is the resistance of the electrolyte solution between the working electrodes and the reference electrode. R_{dl} represents the charge transfer resistance at the metal/electrolyte interface and can be estimated from the diameter of the capacitive loop. The impedance value of a CPE is acquired according to $A^{-1}(i\,\omega)^{-n}$, where A is a constant related to capacitance, i is an imaginary figure, ω is the angular frequency, and n is an exponential factor varying from -1 to 1. CPE can be determined as a resistance, capacitance, inductance, or Warburg impedance in different conditions, with n often ranging from zero to 1 [5, 23, 24]. The attained data from EIS tests in the Table 1 show that the corrosion performance of both samples was close to each other and showed the same order of values, with R_{dl} being about 14010 and 14250 Ω cm^2 for wrought and SLM-fabricated 316L SS, respectively. The CPE_{dl} value for these specimens was achieved about 550 and 530 μF cm^{-2}s^n, respectively. Therefore, one can conclude that the corrosion performance of both samples was close to each other and showed the same order of values.

After 4 weeks of immersion, the corrosion behavior of the specimens showed some variations. Nyquist plots revealed a semi-circle followed by a tail, indicating the Warburg diffusion process. The SLM fabricated 316L SS exhibited higher charge transfer and Warburg resistance value compared to its wrought counterpart. The lower corrosion resistance of the wrought sample after 4 weeks of immersion could be explained by the presence of detrimental phases. R_{dl} for wrought and SLM processed 316L SS was obtained about 2684 and 3307 Ω cm^2, respectively. Besides, CPE_{dl} for these specimens estimated about 480 and 500 μF cm^{-2}s^n, respectively. The Warburg impedance could be caused by the process of migration of metal vacancies and oxygen vacancies within the passive film [23, 25, 26].

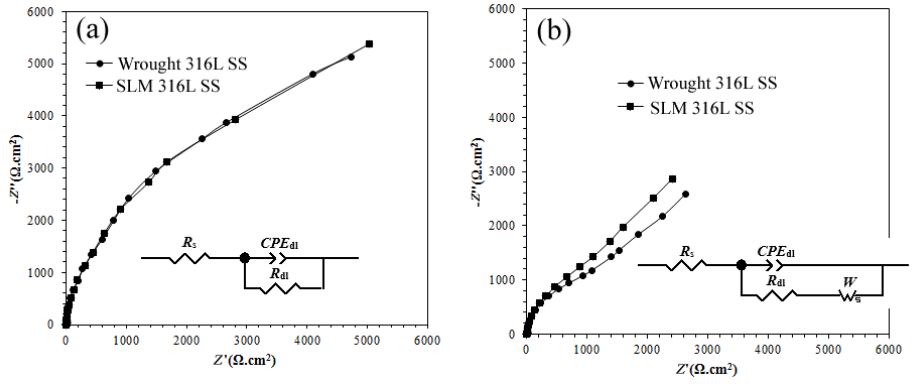

Fig. 4. Nyquist plots of wrought and SLM processed 316L SS in the concrete pore solution for (a) 3 h and (b) 4 weeks of immersion.

Table 1. The obtained electrochemical parameters from ZView simulation regarding the corrosion of wrought and SLM processed 316L SS in the concrete pore solution.

Specimen	Time	R_s, Ω cm^2	CPE_{dl} μF cm^{-2} s^n	n	R_{dl} Ω cm^2	W-R, Ω cm^2	χ^2
Wrought 316L SS	3 h	1.43	550	0.94	14010	-	0.001
SLM 316L SS	3 h	1.49	530	0.93	14250	-	0.002
Wrought 316L SS	4 w	0.98	480	0.89	2684	5823	0.001
SLM 316L SS	4 w	0.81	500	0.9	3307	8500	0.004

The potentiodynamic polarization measurements of the wrought and SLMed alloys in concrete pore solution are shown in Fig. 5. The corrosion parameters of the two specimens are provided in Table 2. It can be seen that the corrosion current density of the wrought sample is approximately three times higher than that of the SLM-fabricated sample, measuring at 9.6 μA cm^{-2}. Additionally, the ipass value for the SLMed alloy is about one-fifth of its counterpart, indicating a greater ability of the SLM-fabricated alloy to exhibit passivation behavior.

The image in Fig. 6. shows the appearance of the samples after being submerged in the concrete pore solution. When comparing the SLM sample surface (Fig. 6b.) to the wrought counterpart (Fig. 6a.), it can be observed that the SLM sample has more areas that remain intact. This suggests that the SLM sample experienced less corrosion damage while being immersed in acidic media [20, 27].

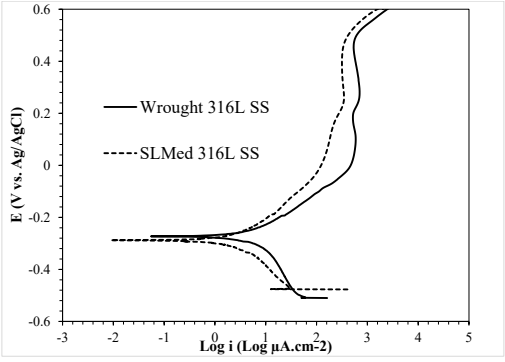

Fig. 5. Potentiodynamic polarization tests regarding wrought and SLM-fabricated alloys in the concrete pore solution.

Table 2. Corrosion parameters obtained from dynamic polarization of wrought and SLM-fabricated 316L SS in the concrete pore solution.

Sample	E_{corr}, mV vs. Ag/AgCl	i_{corr}, μA cm^{-2}	β_c, decade	β_a, decade	E_{pass}, mV vs. Ag/AgCl	i_{pass}, μA cm^{-2}	E_{pit}, mV vs. Ag/AgCl
wrought	-273	9.6	0.21	0.24	2	467	495
SLMed	-288	3.6	0.19	0.29	-4	100	473

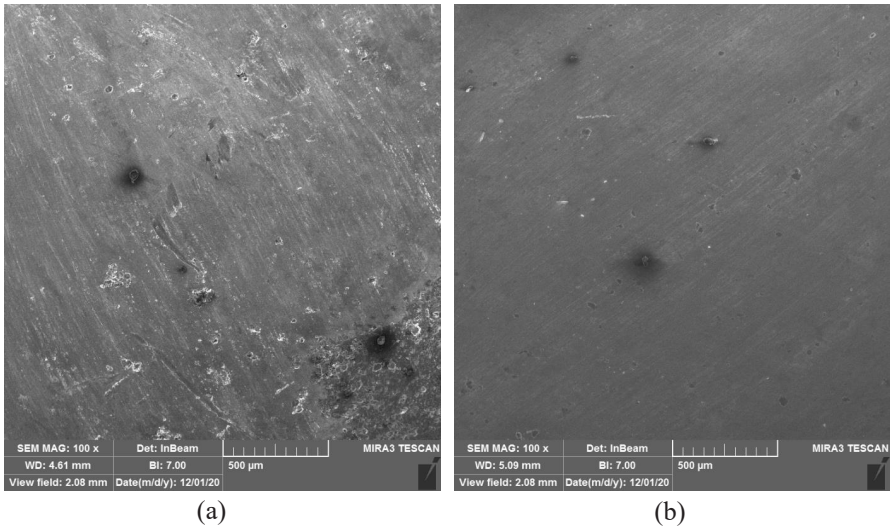

(a) (b)

Fig. 6. Surface morphology after corrosion(a) wrought sample, and (b) SLM-fabricated sample.

4. Conclusions

The present study aimed to investigate the electrochemical behavior of Selective Laser Melting (SLM) processed 316L stainless steel (SS) in comparison to its wrought counterpart when exposed to the concrete pore solution. It was observed that the SLM process had the ability to alter the microstructure and electrochemical properties of the stainless steel. The SLM specimen exhibited cellular/columnar grains with a sub-grain structure with sub-micron sizes. Electrochemical tests conducted after a 4-week immersion period indicated that the SLM-fabricated stainless steel displayed higher corrosion resistance and lower current density compared to the wrought counterpart. Furthermore, the rapid cooling rate associated with the SLM process effectively prevented the formation of detrimental phases, such as TiN, which are known to negatively impact corrosion performance and surface integrity.

5. Acknowledgement

This research was financially supported by Shahid Chamran University of Ahvaz with the Grant Number of SCU.EM1401.31395.

References

[1] Miller J.T, Martin H.J, Cudjoe E, Comparison of the effects of a sulfuric acid environment on traditionally manufactured and additive manufactured stainless steel 316L alloy. Addit Manuf. 2018; 23: 272–86.
[2] Suryawanshi J, Baskaran T, Prakash O, Arya SB, Ramamurty U, On the corrosion resistance of some selective laser melted alloys, Materialia. 2018; 3: 153–61.
[3] Kaladhar M, Venkata Subbaiah K, Srinivasa Rao C.H, Machining of austenitic stainless steels - A review, Int J Mach Mach Mater. 2012; 12(1–2): 178–92.
[4] Zhao Y, Wu A.P, Yao W, Wang Z.M, Sato YS, Kokawa H, Microstructure and mechanical properties of Nd: YAG laser welded invar 36 alloy. Mater Sci Forum. 2011; 675–677: 739–42.
[5] Moghadas S.M.J, Yeganeh M, Zaree S.R.A, Eskandari M, Influence of low temperature heat treatment on microstructure, corrosion resistance and biological performance of 316L stainless steel manufactured by selective laser melting, CIRP J Manuf Sci Technol. 2023; 40: 68–74.
[6] Mohammadali S, Moghadas J, Yeganeh M, Reza S, Zaree A, Eskandari M, The influence of heat treatment on the microstructure and corrosion behavior of selective laser melted 316L stainless steel in Ringer's solution The in fl uence of heat treatment on the microstructure and corrosion behavior of selective laser melted 316, Surf Topogr: Metrol Prop. 2022; 10: 025012.
[7] Soleimani S, Yeganeh M, Lari Baghal S.M, Electrochemical behavior of laser powder bed fusion fabricated 316L stainless steel in a nitric acid solution, J Laser Appl. 2022; 34(4): 042036.
[8] Krakhmalev P, Yadroitsava I, Fredriksson G, Yadroitsev I, In situ heat treatment in selective laser melted martensitic AISI 420 stainless steels. Mater Des. 2015; 87: 380–5.
[9] Parry L, Ashcroft I.A, Wildman R.D, Understanding the effect of laser scan strategy on residual stress in selective laser melting through thermo-mechanical simulation, Addit Manuf. 2016; 12: 1–15.
[10] Bartolomeu F, Sampaio M, Carvalho O, Pinto E, Alves N, Gomes J.R, et al. Tribological behavior of Ti6Al4V cellular structures produced by Selective Laser Melting, J Mech Behav Biomed Mater. 2017; 69: 128–34.
[11] Zhao X, Wei Q, Song B, Liu Y, Luo X, Wen S, et al. Fabrication and Characterization of AISI 420 Stainless Steel Using Selective Laser Melting, Mater Manuf Process. 2015; 30(11): 1283–9.
[12] Song B, Zhao X, Li S, Han C, Wei Q, Wen S, et al. Differences in microstructure and properties between selective laser melting and traditional manufacturing for fabrication of metal parts: A review. 2015; 10: 111–25.
[13] Zhong Y, Liu L, Wikman S, Cui D, Shen Z, Intragranular cellular segregation network structure strengthening 316L stainless steel prepared by selective laser melting, J Nucl Mater. 2016; 470: 170–8.
[14] Tucho W.M, Lysne V.H, Austbø H, Sjolyst-Kverneland A, Hansen V, Investigation of effects of process parameters on microstructure and hardness of SLM manufactured SS316L. J Alloys Compd. 2018 Apr; 740: 910–25.
[15] Chao Q, Cruz V, Thomas S, Birbilis N, Collins P, Taylor A, et al. On the enhanced corrosion resistance of a selective laser melted austenitic stainless steel, Scr Mater. 2017; 141: 94–8.
[16] Lodhi M.J.K, Deen K.M, Haider W, Corrosion behavior of additively manufactured 316L stainless steel in acidic media, Materialia. 2018; 2: 111–21.
[17] Lodhi M.J.K, Deen K.M, Greenlee-Wacker M.C, Haider W, Additively manufactured 316L stainless steel with improved corrosion resistance and biological response for biomedical applications, Addit Manuf. 2019; 27: 8–19.
[18] Muley S.V, Vidvans A.N, Chaudhari G.P, Udainiya S, An assessment of ultra fine grained 316L stainless steel for implant applications, Acta Biomater. 2016; 30: 408–19.
[19] Shaeri Karimi M.H, Yeganeh M, Alavi Zaree S.R, Eskandari M, Corrosion behavior of 316L stainless steel manufactured by laser powder bed fusion (L-PBF) in an alkaline solution, Opt Laser Technol. 2021; 138: 106918.
[20] Yeganeh M, Rezvani M.H, Laribaghal S.M, Electrochemical behavior of additively manufactured 316 L stainless steel in H2SO4 solution containing methionine as an amino acid. Colloids Surfaces A Physicochem Eng Asp. 2021; 627: 127120.

[21] Tiamiyu A.A, Eduok U, Szpunar J.A, Odeshi A.G, Corrosion behavior of metastable AISI 321 austenitic stainless steel: Investigating the effect of grain size and prior plastic deformation on its degradation pattern in saline media, Sci Rep. 2019; 9(1).
[22] Shahryari Z, Gheisari K, Yeganeh M, Ramezanzadeh B, MoO4 2−-doped oxidative polymerized pyrrole-graphene oxide core-shell structure synthesis and application for dual-barrier & active functional epoxy-coating construction, Prog Org Coatings. 2022; 167: 106845.
[23] Shoushtari M.T, Yeganeh M, Kotoki D.G, Enhanced corrosion resistance of 17-4 PH stainless steel fabricated by laser powder bed fusion in H2SO4 solution, J Laser. 2022; 34(2): 022023.
[24] Salehi M, Yeganeh M, Heidari R.B, Eskandari M, Comparison of the microstructure, corrosion resistance, and hardness of 321 and 310s austenitic stainless steels after thermo-mechanical processing, Mater Today Commun. 2022; 31: 103638.
[25] Saremi M, Yeganeh M, Application of mesoporous silica nanocontainers as smart host of corrosion inhibitor in polypyrrole coatings, Corros Sci. 2014; 86: 159–70.
[26] Yeganeh M, Shoushtari M.T, Jalali P, Evaluation of the corrosion performance of selective laser melted 17-4 precipitation hardening stainless steel in Ringer's solution, J Laser Appl. 2021; 4: 042001.
[27] Yeganeh M, Khosravi-Bigdeli I, Eskandari M, Zaree S.R.A, Corrosion Inhibition of L-Methionine Amino Acid as a Green Corrosion Inhibitor for Stainless Steel in the H2SO4 Solution, J Mater Eng Perform. 2020; 29: 3983–94.